Environmental Science and Pollution Research (2020) 27:15337–15349
https://doi.org/10.1007/s11356-020-08046-2

RESEARCH ARTICLE

Advanced landfill leachate biochemical effluent treatment using Fe-Mn/AC activates $O_3/Na_2S_2O_8$ process: process optimization, wastewater quality analysis, and activator characterization

Zhanmeng Liu[1] · Liang Pan[1] · Fengping Hu[1] · Yunqi Hu[1]

Received: 14 July 2019 / Accepted: 10 February 2020 / Published online: 19 February 2020

Abstract

A novel catalyst of Fe-Mn/AC was prepared and used as a heterogeneous catalyst to activate $O_3/Na_2S_2O_8$ for landfill leachate biochemical effluent treatment. The experimental results indicated that the highest COD (84%) and color (98%) removal was obtained at Fe-Mn/AC dosage 1.2 g/L, O_3 concentration 1.2 g/L, $Na_2S_2O_8$ dosage 6 g/L, initial pH 10, and reaction time 100 min. Three-dimensional and excitation emission matrix (3D-EEM) fluorescence spectrometry, Fourier transform infrared spectroscopy (FTIR), and gas chromatography mass spectrometry (GC/MS) of wastewater samples before and after treatment demonstrated that the leachate biochemical effluent contained a large amount of humic and fulvic acid organic compounds. After treatment with this coupling system, both the pollution level of dissolved organic matter (DOM) and the fluorescence intensity declined. The micro morphology of Fe-Mn/AC was characterized using scanning X-ray diffraction patterns (XRD), electron microscope spectra (SEM), X-ray photoelectron spectroscopy (XPS), and Fourier transform infrared (FTIR) spectroscopy. It can be concluded that the microscopic morphology of the catalyst is porous. The main active components are amorphous MnO_2 and multivalent iron oxides. Furthermore, the Fe-Mn/AC catalyst showed great reusability; the removal efficiency of COD was only reduced from 84% to 79% at the fourth reaction. Moreover, the COD removal efficiency could recover to 81% after catalyst regeneration.

Keywords Activator characterization · Fe-Mn/AC · Leachate biochemical effluent · Reusability · Sulfate radical oxidation · Spectrum analysis

Introduction

Sanitary landfill is widely applied as the most common technique in the management of municipal solid waste due to its low cost and simple operation (Calabrò et al. 2015, 2018; Renou et al. 2008). However, a major issue associated with solid waste landfilling is the generation of leachate (Clarke et al. 2015). Landfill leachates are high-strength polluted wastewaters characterized by high concentrations of toxic and carcinogenic chemicals (Amor et al. 2015; Ma et al. 2018; Stefania et al. 2018). Therefore, landfill leachate should be treated efficiently in order to eliminate the potential for the pollution of ground water and surface water. In practice, the treatment of landfill leachate continues to be a thorny problem (Postacchini et al. 2018). Biological degradation is the most prevalent technology used for the treatment of landfill leachate due to its low cost (Ahmed and Lan 2012; Chemlal et al. 2014). However, biological degradation alone cannot treat landfill leachate efficiently, and the effluent does not always meet the national discharge standards (Kumiawan et al. 2006). After treatment with a biological process, there are still many residual persistent pollutants in the leachate effluent (Abood et al. 2014) which require further treatment. The treatment of leachate biochemical effluent is a significant challenge because of its residual persistent pollutants.

Advanced oxidation processes (AOPs) have been widely applied in the treatment of wastewater containing different organic compounds that are non-biodegradable or toxic to microorganisms. Typical AOP systems for leachate treatment have been widely studied including electro catalytic oxidation

Responsible editor: Vítor Pais Vilar

✉ Zhanmeng Liu
ustblzm@sina.com

[1] School of Civil Engineering and Architecture, East China Jiao Tong University, 808 East Shuanggang Road, Nanchang 330013, China

(Feng and Li 2003), wet air oxidation (Zhou et al. 2018), ozonation (Broséus et al. 2009), Fenton (Tusar et al. 2012), or Fenton-like oxidation (Bokare and Choi 2014), as well as various combinations of these systems. The use of ozone alone for leachate treatment has the disadvantages of low removal efficiency and insufficient oxidizing capacity (Amr et al. 2013). However, the use of UV/O_3 (Nawrocki and Fijołek 2013), O_3/H_2O_2 (Bourgin et al. 2017), $UV/O_3/H_2O_2$ (Cortez et al. 2010), and other methods combined with ozone treatment of leachate can significantly increase the reaction efficiency and oxidative degradation ability.

In recent years, persulfate ($S_2O_8^{2-}$) has drawn increasing attention as an alternative for the oxidation of contaminants and is considered promising (Devi et al. 2016). $S_2O_8^{2-}$ itself is a strong oxidant with a standard oxidation potential ($E°$) of 2.01 V (Matzek and Carter 2016). Furthermore, $S_2O_8^{2-}$ can be activated to form a powerful sulfate radical (SO_4^{-}, $E° = 2.6$ V) by heat (Miao et al. 2018), transition metals (Gao et al. 2018), UV light (An et al. 2015), and so on. It has been demonstrated by related studies that a broad spectrum of organic pollutants can be rapidly degraded using $SO_4^{-}\cdot$ oxidation (Yang and Ezyske 2011). The advanced oxidation process based on sulfate radicals has strong oxidative capacity and low cost, which facilitate its potential application in wastewater treatment.

It is well known that the O_3/H_2O_2 advanced oxidation process has a wide range of applications in water and wastewater treatment (Zhao et al. 2017). Similar to H_2O_2, there is also a –O–O– bond in the structure of persulfate. Considering the similar structure of H_2O_2 and $S_2O_8^{2-}$, the $O_3/Na_2S_2O_8$ oxidation system should have similar oxidation characteristics. Experimental studies (Urs 2003) have shown that when ozone gas is introduced into persulfate solution, $S_2O_8^{2-}$ can be activated to produce $SO_4^{-}\cdot$; at the same time, a large amount of ·OH is produced, which further enhances the degradation of organic pollutants (Eqs. 1~6).

$$O_3 + OH^- \rightarrow HO_2^- + O_2 \quad (1)$$

$$O_3 + HO_2^- \rightarrow HO_2^- + O_3^- \quad (2)$$

$$O_3 + H_2O \rightarrow \cdot OH + O_2 + OH^- \quad (3)$$

$$S_2O_8^{2-} + \cdot OH \rightarrow HSO_4^- + SO_4^- \cdot + 1/2O_2 \quad (4)$$

$$SO_4^- \cdot + \cdot OH \rightarrow HSO_4^- + 1/2O_2 \quad (5)$$

$$SO_4^- \cdot + OH^- \rightarrow SO_4^{2-} + \cdot OH \quad (6)$$

In addition, the use of a catalyst can further improve the removal efficiency. Some studies have shown that the application of heterogeneous metal catalysts to catalyze oxidant for treatment of wastewater cannot only effectively improve the removal of pollutants, but also reduce the dosage of oxidant (Akhtar et al. 2011; Keykavoos et al. 2013; Zhang et al. 2018). Moreover, compared with the homogeneous catalyst, the heterogeneous metal catalyst can be effectively separated from the reaction system and does not cause secondary pollution to the wastewater (Liu et al. 2017). Among the various heterogeneous metal catalysts studied, Fe and Mn have been widely used due to their easy availability, stable properties, and high catalytic activity (Jo et al. 2014). Saputra and his coworkers (Saputra et al. 2013) have used three different heterogeneous metal catalysts (Mn_3O_4, Co_3O_4, and Fe_3O_4) to catalyze persulfate treatment of phenol-containing wastewater. Under the optimal reaction conditions, 25 mg/L of phenol could be completely removed after 20 min.

In this study, a novel catalyst of Fe-Mn/AC was prepared and used as a heterogeneous catalyst to activate $O_3/Na_2S_2O_8$ for the generation of SO_4^{-}. This was used to oxidize the residual pollutants in the leachate biochemical effluent, and the related experimental parameters were optimized. The wastewater sample, before and after treatment with the Fe-Mn/AC catalytic $O_3/Na_2S_2O_8$ system, was analyzed using 3D-EEM, FTIR, and GC-MS. The Fe-Mn/AC was characterized by XRD, SEM, XPS, and FTIR, before and after use. The reuse and regeneration of the Fe-Mn/AC catalyst were also investigated.

Materials and methods

Leachate sampling

Leachate samples were obtained from Maiyuan refuse landfill of Nanchang, China. The samples were put in acid-pre-treated polyethylene bottles, transported to the laboratory, and then stored at 4 °C. General characteristics of the leachate are shown in Table 1.

Fe-Mn/AC preparation

Activated carbon pretreatment The activated carbon selected in this study was purchased from Stace Carbon Corporation (Nanchang). Before the experiment, the activated carbon was cleaned by ultrasonic for 1 h and then washed with distilled water. Finally, the pre-treated activated carbon was dried at 80 °C and stored in a desiccator.

Preparation of the Fe-Mn/AC catalyst Briefly, a mixture contains $KMnO_4$ and $FeNO_3 \cdot 9H_2O$, with a molar ratio of Fe^{3+} to Fe^{2+} of 2:1. Then, it was stirred for 1 h at 60 °C in a water bath thermostat magnetic stirrer (stirring speed was medium). During this process, NaOH solution was added to keep the pH in the range 7~8. This was stirred for 12 h and then filtered. Then, the residue was washed several times with distilled water, dried, and ground to obtain iron and manganese oxide. An appropriate amount of the dried and ground iron and manganese oxide was added to distilled water along with the pretreated activated carbon. Then, oscillatory impregnation

Table 1 Main water quality indicators for wastewater

Color/ times	pH	COD/mg/ L	BOD_5	NH_3-N/mg/ L	TS/mg/L
650–750	5–6	1000–1400	300–400	100–150	260
Cd^{2+}/μ/L	As^{3+}/μg/L	Hg^{2+}/μg/L	Cr^{3+}/μg/L	Cr^{6+}/μg/L	Pb^{2+}/μg/L
0.05	1.42	0.04	0.39	0.03	0.09

was performed for 8–10 h to make sure the iron and manganese oxide were fully loaded onto the activated carbon. Finally, the mixture was dried, placed in muffle furnace, heated at 3 °C/min to 450 °C, and calcined for 2 h. The calcined product was Fe-Mn/AC catalyst.

Catalytic oxidation experiment

As shown in Fig. 1, the system included an oxygen tank, bubble stone, ozone generator (HY-001-5A, Guangzhou Jiahuan Electric), and a reactive column made of Plexiglas, the cover of which could be moved. Moreover, the pipes connecting various parts of the reaction column were all of PVC. In addition, ozone gas generated by the ozone generator is introduced into the reaction column through the bubble stone at the bottom of the reactor, and the off-gas produced by the reaction was absorbed by KI solution.

The single factor control variable method was used to study the influence of each factor to obtain an optimal experimental condition. First, using 0.1 mol/L sulfuric acid or sodium hydroxide solution to adjust the solution pH to the desired values (3, 4, 5, …, 11). Second, the wastewater containing a certain concentration of persulfate (1, 2, 3, …, 8 g/L) leachate was introduced into the reaction column through the peristaltic pump. At the same time, a certain amount of Fe-Mn/AC catalyst (0.2, 0.4, 0.6, …, 1.6 g/L) was added. Next, turn on the ozone generator and adjust the output of ozone (0.2, 0.2, 0.3, …, 1.6 g/L). Last, a sample was taken from the sampling port for analysis after the reaction had proceeded for a certain time.

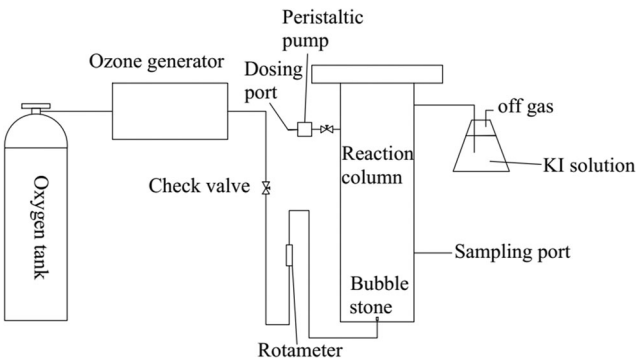

Fig. 1 Schematic diagram of the experimental apparatus

Spectrum analysis of a wastewater sample

3D-EEM fluorescence spectra

The excitation emission matrix (EEM) fluorescence was determined using a fluorescence spectrophotometer (Hitachi F-2000). Referring to literature (Zhu et al. 2012) and optimizing experiment many times, scanning parameters were set as follows: excitation wavelength: 220–500 nm, scan wavelength intervals: 20 nm, slits: 10 nm; emission wavelength: 250–600 nm, scan wavelength speed: 1200 nm/min, slits: 10 nm; the voltage of photomultiplier: 700 V, the illuminant of excitation: 150 W xenon arc lamp, response time: automatic.

FTIR spectroscope

The wastewater samples were analyzed by FTIR spectrophotometer (Mohamed et al. 2017) (model D/Max-RC). Briefly, the wastewater samples before and after treatment were dried and mixed with pre-dried KBr powder, respectively, and then were both sufficiently ground and pressed in a pellet which was suitable for FTIR analysis. FTIR spectroscopy was then conducted and the spectra were in the range of 4000–400 cm^{-1}.

GC-MS spectrometry

Water sample pretreatment To extract as much trace organic matter as possible from the leachate, 500 mL of leachate was extracted twice in CH_2Cl_2 under neutral, basic, and acidic conditions. The organic phases extracted under neutral, alkaline, and acidic conditions were combined and the water in the extract was absorbed using with anhydrous sodium sulfate. A rotating evaporator was used to inject 2–3 mL of sample concentrate into chromatographic column at 45 °C. First, the nonpolar organic matter was eluted with n-hexane; then, the aromatic hydrocarbons were eluted with benzene. Finally, the remaining organic substances (such as polar phenols) were eluted with ethanol. These were concentrated separately to about 1 mL for later use. The landfill leachate was analyzed using gas chromatography-mass spectrometry (Agilent 7890A-5975C) before and after treatment. The GC oven temperature was kept at 60 °C; then programmed to reach 260 °C at 5 °C/min. The temperature was kept constant at 260 °C for

40 min. A split/splitless injector was used in splitless mode and the injector temperature was 250 °C. Mass spectrographs were taken at 70 eV in EI mode. The mass range was between m/z 30 and 425 (Zhang et al. 2013).

Microscopic morphological characterization of Fe-Mn/AC

XRD patterns

To determine the crystalline phases, the Fe-Mn/AC was analyzed using XRD with an X-ray diffractometer (model D/Max-RC, Japan) and with Cu-Ka radiation in the 2θ range of 5.00–79.98° at a scan rate of 6°/min.

SEM micrograph

The surface morphology of the Fe-Mn/AC was determined using SEM (model S-3400 N II/HORIBAEX-250, Japan). The samples were prepared as follows. A small amount of sample was fixed on a sample stub using conductive carbon glue, then pressed flat, and dried on a heating plate. An ion sputter apparatus was used to coat the surface of the sample with platinum to a thickness of 30 A.

XPS spectra

XPS spectra were produced using a Kratos AXIS Ultra DLD system (Kratos Analytical, Manchester, United Kingdom), equipped with Al Ka radiation (hv = 1486.6 eV). It is convenient to record XPS spectra after cleaning each specimen using Ar to etch (5 kV, 20 mA) the surface. The analyzer was fixed perpendicular to the sample surface with a detection angle of 45° and operated at the constant-pass energy of 20 eV. In addition, the step size was set at 0.02 eV and each peak was scanned twice to ensure the acquisition of high-resolution spectra.

FTIR spectroscopy

The functional groups and structure of the Fe-Mn/AC catalyst were using a Spectrum OneNTS Fourier transform infrared spectrometer. Regarding the specific operation method (Mohamed et al. 2017), at normal temperature, a small amount of pre-dried catalyst and excess KBr were carefully ground on an agate mortar. For testing, the powder was pressed for 3–5 min under a certain pressure to form a sheet; then, the related spectra were measured and used a Fourier spectrometer. The data were imported into Origin software for drawing and analysis.

Results and discussion

Treatment of leachate biochemical effluent with the Fe-Mn/AC catalytic $O_3/Na_2S_2O_8$ system

Effect of $Na_2S_2O_8$ dosage on COD and color removal

It is seen from Fig. 2 that a higher $Na_2S_2O_8$ dosage generally favored COD and color removal. The COD and color removal efficiency first gradually increased with $Na_2S_2O_8$ dosage from 1 to 6 g/L. When the $Na_2S_2O_8$ dosage was 6 g/L, the removal efficiency of COD and color reached 84% and 98%, respectively, which was significantly changed from that of low-dose persulfate reaction. The reason for this might be that with the increasing dosage of $Na_2S_2O_8$, on the one hand, the collision probability between persulfate and metal ions on activated carbon increases. This results in a large number of –O–O– cleavage in the $S_2O_8^{2-}$ to generate $SO_4^{-}\cdot$ (Lee et al. 2010); on the other hand, ozone can produce ·OH, and then, ·OH can activate $S_2O_8^{2-}$ and cause it to decompose rapidly to generate $SO_4^{-}\cdot$ (Eqs. 3 and 5) (Soubh and Mokhtarani 2016; Urs 2003); so, the removal efficiency of COD in the solution increases. However, when the $Na_2S_2O_8$ dosage was further increased, the oxidation effect was inhibited and the removal efficiency of COD and color did not improve. There are two main reasons for this: (1) excessive $SO_4^{-}\cdot$ quenches itself (Eq. 7), making the $S_2O_8^{2-}$ concentration decrease (Li et al. 2013), and (2) excessive $S_2O_8^{2-}$ also reacts with $SO_4^{-}\cdot$ and consumes $SO_4^{-}\cdot$ reactive groups in solution (Eq. 8) (Dhaka et al. 2017; Salari et al. 2009).

$$SO_4^{-}\cdot + SO_4^{-}\cdot \rightarrow S_2O_8^{2-} \quad (7)$$

$$SO_4^{-}\cdot + S_2O_8^{2-} \rightarrow SO_4^{2-} + S_2O_8^{-} \quad (8)$$

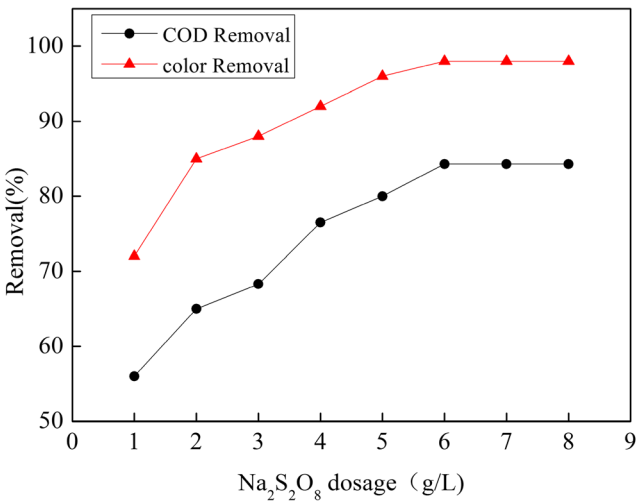

Fig. 2 Effect of $Na_2S_2O_8$ dosage on the COD and color removal (Fe-Mn/AC dosage = 1.2 g/L, O_3 concentration = 1.2 g/L, pH = 10.0, reaction time = 120 min)

Effect of ozone concentration on COD and color removal

As is seen from Fig. 3, the change in the ozone concentration has great influence on the oxidation effect. When ozone concentration increased from 0.2 to 1.2 g/L, the COD removal efficiency was significantly improved from 52.6 to 84%. The main reason might be that as the concentration of ozone increases, more ozone molecules react with the catalyst and continue to generate ·OH. At the same time, ·OH reacts rapidly with organic compounds due to its strong oxidizing and non-selective properties. On the other hand, ·OH can activate $S_2O_8^{2-}$ and cause it to decompose rapidly to generate SO_4^{-}·. This strengthens the ability to degrade organic substances, and the removal efficiency of COD is effectively improved. However, when ozone concentration exceeds 1.2 g/L, the removal efficiency of COD and color do not improve, because ozone and organic matter in the wastewater compete for reaction with the ·OH (Forni et al. 1982); thus, the free radical concentration in the solution is reduced. This has a negative effect on the degradation of organic matter.

Effect of Fe-Mn/AC dosage on COD and color removal

A suitable catalytic dosage is necessary for oxidation. Too high and too low catalytic dosage results in an unfavorable oxidation. The effect of the Fe-Mn/AC dosage on oxidation performance is shown in Fig. 4. It is obvious that, as the catalyst dosage increased, the removal efficiency of COD and color improved. Transition metal ions from the catalyst transfer an electron to $S_2O_8^{2-}$ so that the –O–O– in $S_2O_8^{2-}$ breaks to form SO_4^{-}· (Eq. 9). In addition, the catalyst can promote ozone decomposition to produce ·OH and enhance the oxidative degradation of organic matter (Legube and Leitner 1999). In this case, the removal efficiency of COD

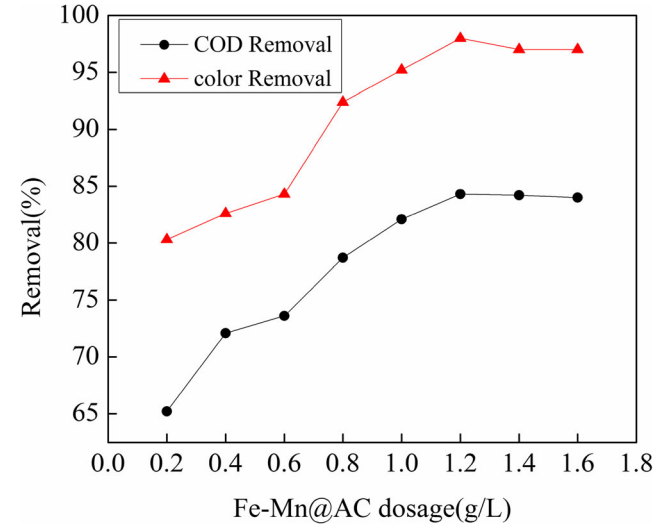

Fig. 4 Effect of Fe-Mn/AC dosage on the COD and color removal (O_3 concentration = 1.2 g/L, $Na_2S_2O_8$ dosage = 6 g/L, pH = 10.0, reaction time = 120 min)

and color increases gradually. When the catalyst in solution was > 1.2 g/L, the removal efficiency of COD did not change clearly and even showed a slight decreasing trend. The reason for this might be that excessive Fe^{2+} reacts with ·OH and SO_4^{-}· to reduce the concentration of SO_4^{-}· and ·OH, thereby reducing the capacity for oxidative degradation of organic pollutants. At the same time, too much Mn^{4+} is oxidized by ozone to a higher valence state, after which it consumes dissolved ozone in the water. The high-valence Mn^{7+} has poor ability to oxidize organic matter (Nawaz et al. 2016).

$$S_2O_8^{2-} + Mn^{+} \rightarrow SO_4^{-}\cdot + SO_4^{2-} + Mn^{(n+1)+} \quad (9)$$

Effect of reaction time on COD and color removal

The effect of reaction time on the oxidation performance is shown in Fig. 5. Both COD and color removal efficiency are

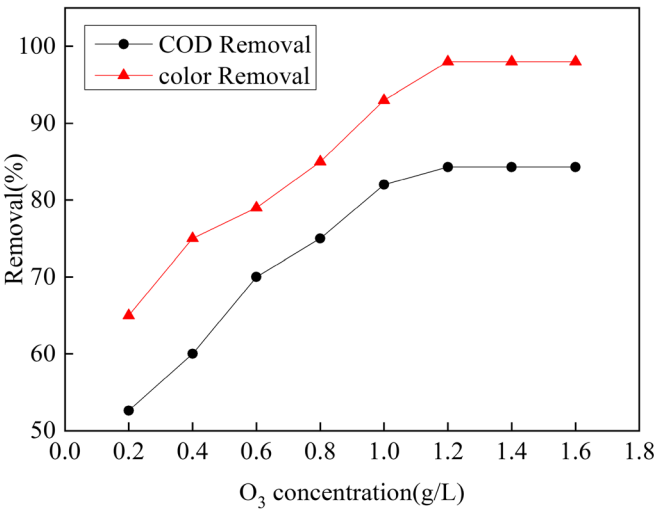

Fig. 3 Effect of O_3 concentration on the COD and color removal (Fe-Mn/AC dosage = 1.2 g/L, $Na_2S_2O_8$ dosage = 6 g/L, pH = 10.0, reaction time = 120 min)

high (84% and 98%, respectively) when the reaction time is 100 min. The removal efficiency remains stable at longer times. This is because organic pollutants consume a large number of ·OH and SO_4^{-}·, so the subsequent degradation ability of this oxidation process is reduced. Moreover, as the reaction proceeds, most of the easily degradable and partially un-degradable soluble organic compounds are completely degraded, while the proportion of refractory organic compounds increases. As a result, the removal efficiency of related indicators no longer rises.

Effect of pH on COD and color removal

As shown in Fig. 6, with increase of the pH, the removal efficiency of COD improved. Under alkaline condition, the removal efficiency of COD is obviously better than in acid condition. In alkaline conditions, the self-decomposition reaction of ozone in the solution is accelerated by OH^{-}, the decomposition of ·OH can react quickly and non-selectively with organic pollutants, and ·OH can activate $S_2O_8^{2-}$ at high pH to produce SO_4^{-}·. This is why the removal efficiency of COD is only 41.2% when pH = 3, but 84% when pH = 10. However, when the wastewater is adjusted to pH 10 and continues to increase, the removal efficiency of COD in the effluent water is not significantly improved. This is mainly because ·OH is the main oxidizing group in the solution. When the pH of the reaction solution is over 10, the activity of ·OH decreases gradually; thus, the degradation ability of organic matter in wastewater is reduced. In addition, it was found in the experiment that the flocculent precipitate appeared in the wastewater under strongly alkaline condition, because the landfill leachate contained a high concentration of calcium ion and the calcium ions that were not completely removed

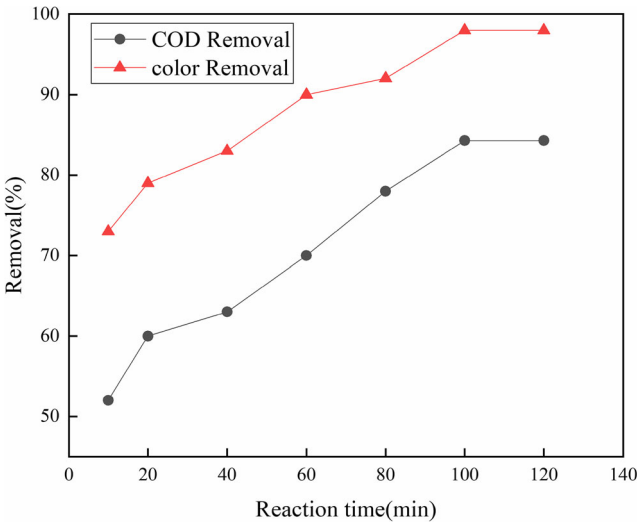

Fig. 5 Effect of reaction time on the COD and color removal (Fe-Mn/AC dosage = 1.2 g/L, $Na_2S_2O_8$ dosage = 6 g/L, O_3 concentration = 1.2 g/L, pH = 10.0)

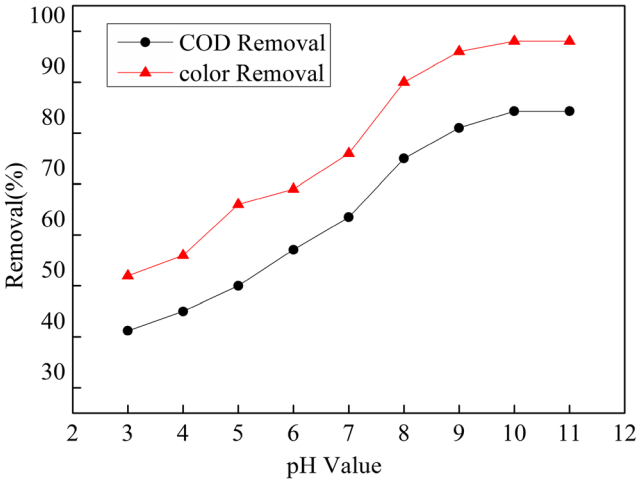

Fig. 6 Effect of pH on the COD and color removal (Fe-Mn/AC dosage = 1.2 g/L, $Na_2S_2O_8$ dosage = 6 g/L, O_3 concentration = 1.2 g/L, reaction time = 120 min)

after the anaerobic-anoxic-aerobic treatment. The residual calcium ions formed $Ca(OH)_2$ precipitate when the wastewater was alkaline, which affected the catalytic oxidation activity of the catalyst. Taking COD and color removal into consideration, it is suggested that pH = 10 would be appropriate for the treatment of this wastewater. It is worth noting that the effluent should be neutralized after treatment to prevent secondary pollution to natural water bodies (Stefania et al. 2018).

Reuse and regeneration of the Fe-Mn/AC catalyst

An important index for evaluating catalyst is whether a catalyst can maintain high activity after repeated use. To investigate the service life of the Fe-Mn/AC catalyst, uniform experimental conditions were set: persulfate dosage 6 g/L, O_3 concentration 1.2 g/L, catalyst dosage 1.2 g/L, and reaction time 120 min. Samples from the same batch of catalyst were used for the tests of catalytic oxidation to determine. Consider the effect of the number of reuses of the catalyst (Fe-Mn/AC) on the degradation of organic matter. The Fe-Mn/AC catalyst was repeatedly washed and dried with deionized water after each use.

As shown in Fig. 7, the Fe-Mn/AC was used, collected, rinsed, dried, and recycled for four times. The COD removal efficiency decreased from 84 to 79% at the fourth catalysis. The concentration of metal ions in the effluent after each treatment was determined using an atomic absorption spectrophotometer. The results showed that only trace iron and manganese ions were eluted after the treatment. The catalyst used four times was washed with deionized water and calcined at 450 °C in a muffle furnace. After calcination, the catalytic activity of the catalyst was restored to a certain extent, and the removal efficiency of COD reaches 81% again. It is suggested that the reason for the decrease in the catalytic activity of the Fe-Mn/AC catalyst after repeated use is not the

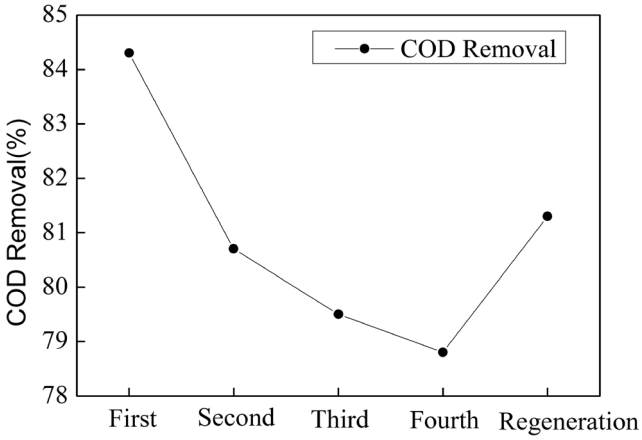

Fig. 7 Reuse and regeneration of Fe-Mn/AC catalyst

overflow of active metal ions, but probably the deposition of small molecules of organic matter or impurities in the activated carbon in the biochemical effluent of the leachate. This hinders the catalytic reaction on the surface of the activated carbon. After calcination, the organic matter was removed and the surface of the activated carbon was improved to a great extent, thus allowing the Fe-Mn/AC catalyst to recover some capacity.

Spectrum analysis of wastewater samples before and after treatment

For this section, the samples of wastewater used for spectrum analysis were all treated under the same conditions: $Na_2S_2O_8$ dosage 6 g/L, Fe-Mn/AC dosage 1.2 g/L, O_3 concentration 1.2 g/L, pH 10, and reaction time at 100 min.

The 3D-EEM fluorescence spectral analysis

Characterization of the molecular structure of benzene rings or organic substances with conjugated double bonds is possible using 3D-EEM fluorescence spectroscopy. In recent years, it has been extensively used in organic structure and transformation analysis. The biochemical tail water of the landfill leachate before and after treatment was subjected to fluorescence tests after 10 times dilution and 0.45-μm filtration. The 3D-EEM fluorescence spectrum analysis is illustrated in Fig. 8. Table 2 shows the changes in the fluorescence index ($f_{450/500}$).

It is observed from Fig. 8 that the DOM of leachate biochemical tail water mainly shows fluorescence characteristic peaks at Ex/Em = 340/410 nm and Ex/Em = 270/540 nm. The corresponding fluorescence intensities were 2159 and 509, respectively. After treatment, the fluorescence characteristic peaks appear mainly at Ex/Em = 300/380 nm and Ex/Em = 270/540 nm. The fluorescence intensities are 165 and 373, respectively. According to research data (Baker 2002; Leenheer and Jean-Philippe 2003), Ex/Em = 340/410 nm and Ex/Em = 300/380 nm

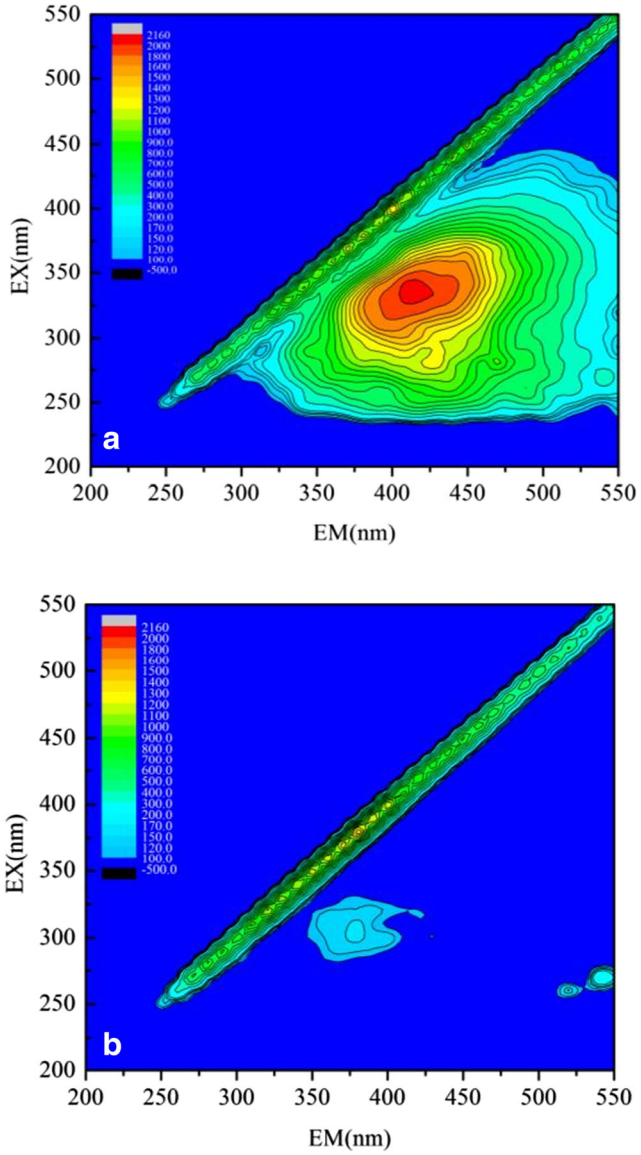

Fig. 8 3DEEM of water samples before (**a**) and after (**b**) treatment

indicate substances in the humic acid-like fluorescent region, and Ex/Em = 270/540 nm indicates a substance in the fulvic acid-like fluorescent region.

Based on Fig. 8, it can be seen that the fluorescence peaks of DOM in the biochemical tail water of the landfill leachate are mainly concentrated in the areas of humic and fulvic acid. Moreover, the fluorescence intensity in the fluorescence region of humic acid is high, which indicates that there are many complex and difficult to degrade humic acid substances in the wastewater.

Table 2 Fluorescence index of wastewater before and after treatment

Samples	Before treatment	After treatment
$f_{450/500}$	1.52	3.03

After advanced treatment with Fe-Mn/AC-catalyzed O_3/$Na_2S_2O_8$, the leachate biochemical tailings still have fluorescence peaks in the humic acid-like and fulvic acid-like regions, but the fluorescence intensity of the two regions decreases to a great extent. The intensity of the humic acid fluorescence peak was reduced from 2159 to 168 (degradation reached 92.2%), which means that the main humic acid substances were nearly all completely degraded. The intensity of the fulvic acid fluorescence peak decreased from 509 to 373, which indicated that the oxidation system of O_3/$Na_2S_2O_8$ catalyzed by Fe-Mn/AC had some degradation effect on the fulvic acid compounds in the biochemical tail water of the leachate.

The fluorescence index ($f_{450/500}$) is the ratio of the intensity of the fluorescence emission spectrum between 450 and 500 nm at an excitation wavelength of 370 nm. The size of $f_{450/500}$ has a negative correlation with the aromaticity of fulvic acid in water. The higher the $f_{450/500}$ ratio, the greater the aromaticity of the fulvic acid in water and the fewer benzene ring structure systems (Wolfe et al. 2002). As shown in Table 2, the fluorescence index of the biochemical tail water of the leachate increased from 1.52 to 3.03 after treatment with the Fe-Mn/AC catalytic O_3/$Na_2S_2O_8$ coupling system indicating that the humic acid in the leachate DOM is weakened, the aromatic ring structure is reduced, and the humic acid and fulvic acids are greatly degraded.

FTIR spectroscopy analysis

The FTIR spectra of wastewater samples before and after treatment are shown in Fig. 9. The absorption peak at 3415 cm^{-1} decreased and the absorption peak at 2353 cm^{-1} increased, after treated by Fe-Mn/AC-catalyzed O_3/$Na_2S_2O_8$ systems. This indicated that this oxidation system reacts strongly with O–H on organic molecules in the wastewater, leading to gradual disintegration of the macromolecular organic matter (Liu et al. 2015). After treatment, the bands at 1646 cm^{-1} decrease significantly, indicating that the content with internal conjugated double bonds (C=C, C=O, etc.) decreases. After treatment, the height of the water sample peak at 1385 cm^{-1} decreases, indicating that the partially saturated hydrocarbon group is cracked by sulfate radicals to form organic compounds with relatively low molecular weight (Zheng et al. 2007). The stretching vibration peak at around 1183 cm^{-1} attenuates after oxidation by the system, indicating that the system reacts strongly with the organic matter in the leachate. Similarly, the intensity of the characteristic peak at 620 cm^{-1} is greatly reduced, indicating that the protein content is relatively reduced (Guangxia et al. 2012).

GC-MS analysis

In order to investigate the changes of organic matter in the biochemical tail water of the landfill leachate before and after treatment, in this experiment used, GC-MS scanning was used to detect the type and content of organic matter in the wastewater.

It is seen from Fig. 10 that the absorption peak of the organic matter has a certain degree of decline, and some absorption peaks even disappear. This was likely due to the complex composition of the biochemical effluent in the landfill leachate and to the influence of external conditions such as instrument accuracy. Many types of organic matter could not be determined in the end because of low detection similarity. Therefore, some organic substances with high degrees of matching were selected for analysis.

Using spectrum matching analysis, Table 3 shows some organic compounds before and after treatment. The retention times are 17.652 min, 28.564 min, 36.264 min, and 39.055 min, representing alkenes, benzene, amides, and alcohols, respectively. The results showed that these four organic

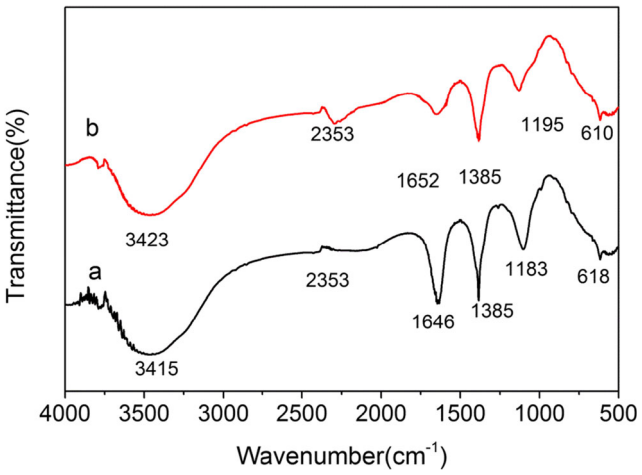

Fig. 9 FTIR spectra of wastewater samples before (**a**) and after (**b**) treatment

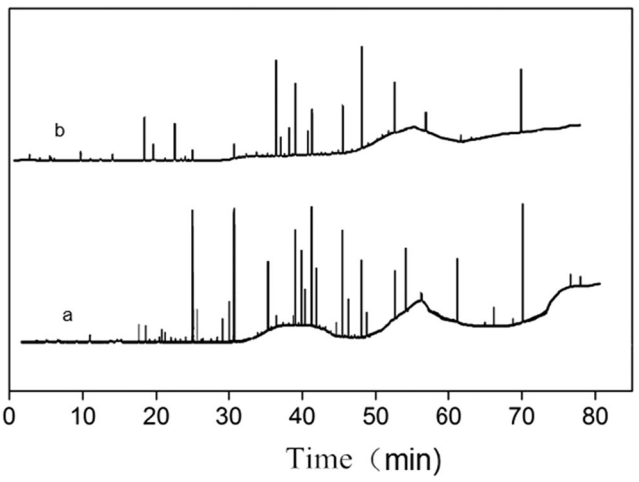

Fig. 10 GC-MS spectra of water samples before (**a**) and after (**b**) treatment

Table 3 GC-MS analysis of wastewater before and after treatment

Number	Retention time (min)	Name of organics	Molecular formula
Before treatment			
1	2.88	Chloroiodomethane	CH_2ClI
2	16.796	2-ethylhexaldehyde	$C_8H_{16}O$
3	17.652	Octamethyltetrasiloxane	$C_6H_{18}O_3Si_3$
4	19.193	3.4.5-trimethyl pyrazole	$C_6H_{11}N_3$
5	21.512	2-ethoxylethyl ether	$C_8H_{18}O_3$
6	22.587	m-Phenylenediamine	$C_6H_4(NH_2)_2$
7	23.308	Triethyl phosphate	$C_6H_{15}O_4P$
8	24.584	Decamethylcyclopentasiloxa-ne	$C_{10}H_{30}O_5Si_5$
9	25.435	4-toluenesulfonyl chloride	$C_7H_7ClO_2S$
10	28.564	(4-methoxy phenyl)-two methylamine	$C_9H_{13}NO$
11	29.104	1,3-dimethyl-2-imidazolidinone	$C_5H_{10}N_2O$
12	30.805	Dodecamethylcyclohexasilo-xane	$C_{12}H_{36}O_6Si_6$
13	33.561	3-ACETAMIDOPHENOL	$C_8H_9NO_2$
14	36.093	5,6-oxy-3-hydroxy-β-ionone	$C_{13}H_2O_3$
15	36.264	4-formyl-N-isopropyl benzoamide	$C_{11}H_{13}NO_2$
16	39.055	cedrol	$C_{15}H_{26}O$
17	40.192	3-(benzoxazole-2-yl) aniline	$C_{13}H_{10}N_2O$
18	40.923	4-phenoxy phenol	$C_{12}H_{10}O_2$
19	41.001	1,3-bis(oxiranylmethyl)-5-(2-propenyl)-1,3,5-Triazine-2,4,6(1H,3H,5H)-trione	$C_{12}H_{15}N_3O_5$
20	41.136	Tetramethylsilane derivative	
21	41.863	3-methoxy phenylthiophenol	$CH_3OC_6H_4SH$
22	41.94	Dimethyl tetradecyl amine	$C_{16}H_{35}$
23	44.69	phytane	$C_{20}H_{43}$
24	45.37	Methyl cyclosiloxane	$C_9H_{24}Si_3$
25	48.489	dibutyl phthalate	$C_{16}H_{22}O_4$
26	49.158	Tetradecamethylhexasiloxn-e	$C_{14}H_{42}O_5Si_6$
27	51.944	Tetradecylamine	$C_{16}H_{35}N$
28	52.634	Tetramethylsilane derivative	
29	55.867	Sixteen methyl seven silox-ane	$C_{16}H_{48}O_6Si_7$
30	71.775	9-octadecene amide	$C_{18}H_{35}$
After treatment			
1	9.874	3-chloropyridine	C_5H_4ClN
2	17.673	Benzyl chloride	C_7H_7Cl
3	19.198	3,4,5-trimethylpyrazole	$C_4H_6N_2$
4	19.8	5-hexyldihydro-2(3H)-furao-ne	$C_{10}H_{18}O_2$
5	21.554	Bromobenzene	C_6H_5Br
6	22.597	4-methyl-1,3-phenylenedia-mine	$C_7H_{11}ClN_2$
7	24.6	Decamethylcyclopentasiloxa-ne	$C_{10}H_{30}O_5Si_5$
8	29.202	2-chloro-3-nitropyridine	$C_5H_3ClN_2O_2$
9	30.811	Dodecylcyclohexylsiloxane	$C_{12}H_{36}O_6Si_6$
10	36.103	Pentadecane	$C_{15}H_{32}$
11	36.228	Dodecyltrimethylammoniu-m bromide	$C_{15}H_{34}NBr$
12	39.066	1-(2-fluorophenyl)piperazin-e	$C_{10}H_{13}FN_2$
13	41.152	3,4-dihydroxyphenyl glycol	$C_8H_{10}O_4$
14	41.946	Dimethyltetradecylamine	$C_{16}H_{35}$
15	44.327	Kusal	$C_{10}H_6Cl_2N_{24}$
16	46.195	Phthalate	$C_8H_6O_4$
17	48.489	Dibutyl phthalate	$C_{16}H_{22}O4$
18	51.949	4-ethylbenzaldehyde	$C_9H_{10}O$
19	71.791	9-octadecenamide	$C_{18}H_{35}$

substances were removed to a higher degree after treatment with the Fe-Mn/AC-catalyzed $O_3/Na_2S_2O_8$.

During treatment, the content of organic substances such as alkene olefins, benzenes, amides, and alcohols was obviously reduced, indicating some of the most toxic or difficult biodegradable organic pollutants. For example, macromolecules with structurally complex rings were opened, disconnected, and degraded into smaller molecules or intermediates. The absorption peak analysis with retention time of 20–30 min may be the

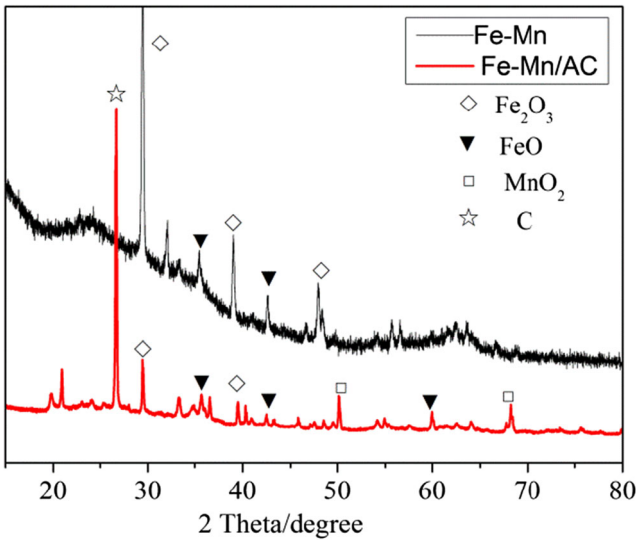

Fig. 11 XRD patterns of the catalyst

product of degradation of macromolecular organic matter.

Characterization and analysis of Fe-Mn/AC

XRD pattern analysis

The XRD patterns of Fe-Mn/AC are shown in Fig. 11. It can be seen that when Fe-Mn is not loaded, the diffraction peak (JCPDs39-0238) of Fe_2O_3 at $2\theta = 29.4°$(022), 39.1°(104), and 48° (113) and that the diffraction peak (JCPDs39-0238) of FeO at $2\ \theta = 35.7°$(111), 42.5°(200), and 60.1° (220). These results show that Fe existed in the form of multivalent states before the activated carbon was loaded. When the iron-manganese compound was loaded onto the activated carbon, the diffraction peak (JCPDs 07-0230) of C was found at $2\theta = 26.7°$ (002), MnO_2 at $2\theta =$ 50.2° (110), and 68.2° (211) from the XRD diagram. Furthermore, there were simultaneous diffraction peaks of Fe_2O_3 at $2\theta = 29.4°$, 39.1°, and 48° (JCPDs 39-0238) and FeO at $2\theta = 35.7°$, 42.5°, and 60.1° (JCPDs 39-0238). It is thus known that activated carbon has been successfully loaded with iron and manganese oxide.

From comparison of the XRD diagram before and after Fe-Mn loading of the activated carbon, it can be seen that the diffraction peak of Fe_2O_3 in the X-ray diffraction pattern is much smaller than before loading. Moreover, the diffraction peak of FeO becomes stronger after the loading. The main reason may be that some metal oxides are decomposed under high-temperature calcination conditions and then reduced to lower oxidation states by reaction with the carbon matrix (Carabineiro et al. 2001). Mn appears as a MnO_2 diffraction peak with low peak strength after loading, but does not appear before loading. This is due to the amorphous form of the manganese oxide before loading, and the loaded MnO_2 is dispersed on activated carbon, which is easier to detect (Yan et al. 2010). In general, after loading, the diffraction peaks of the metal in the XRD diagram are obviously weakened. This also shows that the dispersion of Mn and Fe components loaded on activated carbon is greater than that of Mn and Fe in single-metal supported activated carbon.

SEM micrograph analysis

SEM micrography is commonly used to characterize the structure and morphology of reagents (Hu et al. 2017). The SEM micrographs of nano-Fe_3O_4 (before and after reaction) are shown in Fig. 12. Scanning electron microscopy (SEM) images of the catalysts show that their surfaces have a large number of pore structures. A large number of snowflake-like objects appear on the surface of the activated carbon, which are Fe_3O_4, MnO_2, or other substances. This indicates that the metal oxide was successfully loaded onto the activated carbon, which is consistent with the XRD analysis results. Moreover, it can be seen from the figure that a large amount of metal oxide is dispersed unevenly on the surface of the activated carbon and inside the activated carbon pores. This phenomenon is mainly due to the use of impregnation methods of preparation.

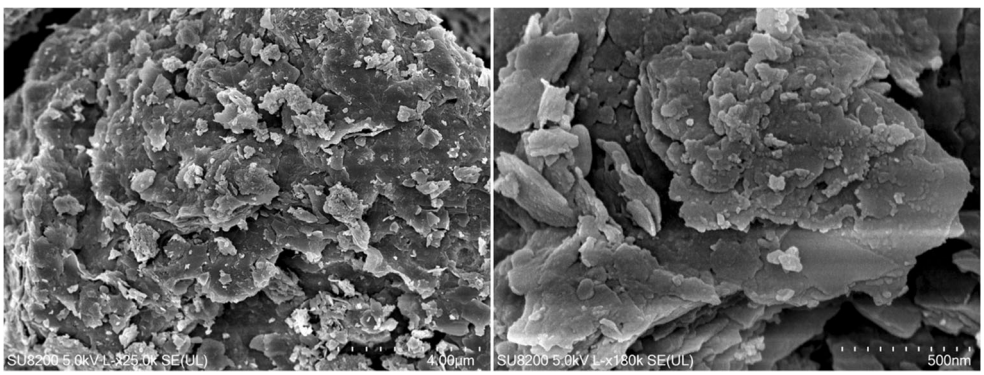

Fig. 12 SEM of Fe-Mn/AC catalyst

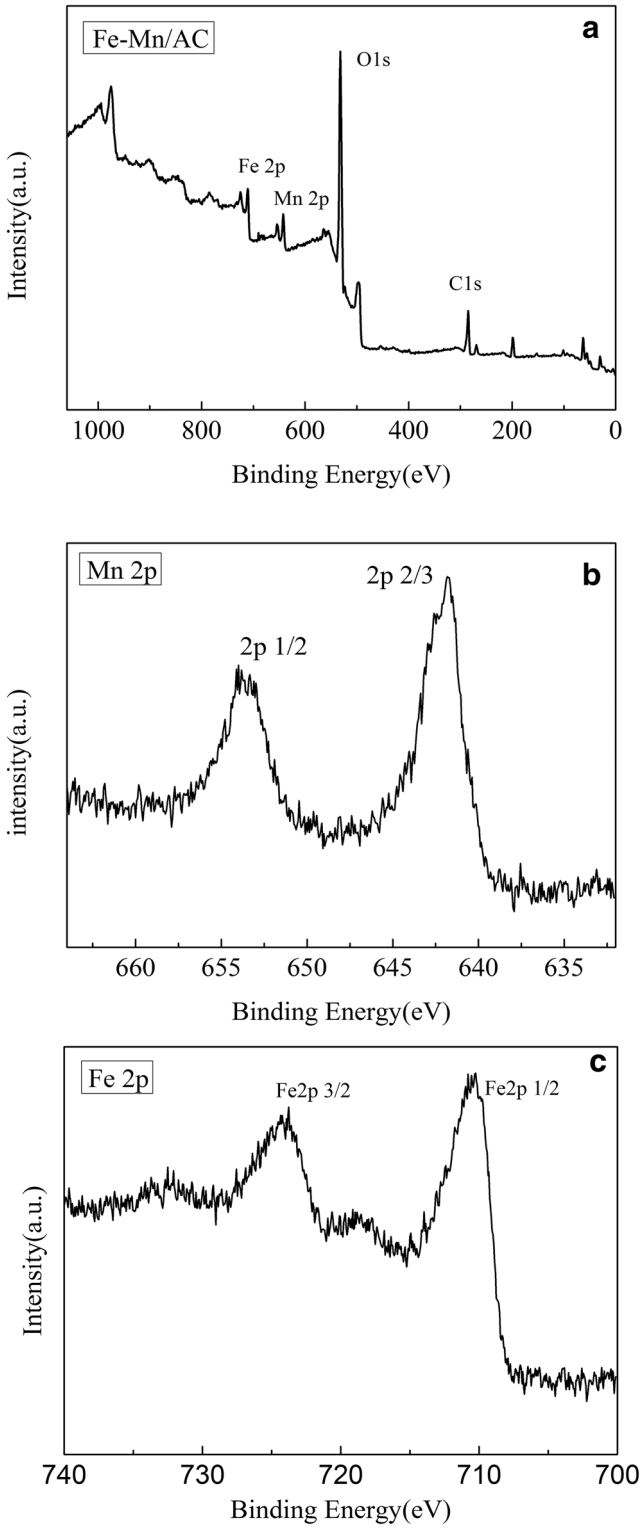

Fig. 13 XPS spectrum of the Fe-Mn/AC catalyst

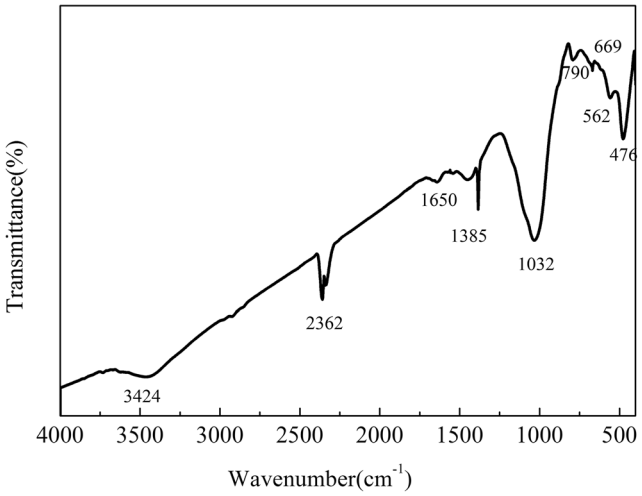

Fig. 14 FT-IR spectra of the Fe-Mn/AC catalyst

XPS spectrum analysis

XPS can detect the elements and atomic valence states on the surface of the material to be characterized over a large energy range at low resolution. It is usually employed to understand changes, not only in the elemental composition and chemical state, but also in the surface structure. The Fe-Mn/AC catalysts were characterized using XPS, and the binding energy was calibrated using the C1s signal (284.6 eV) and oxygen (531.6 eV) C1 signals on the surface of each activated carbon catalyst coating.

In Fig. 13, the XPS characterization diagram for the Fe-Mn/AC catalyst and the corresponding peaks of Fe-2p and Mn-2p are obvious. It can be seen that both Fe and Mn have been successfully loaded on the surface of the activated carbon and exist mainly in the form of their metal oxides. Mn2p XPS spectra have two main binding energy peaks at 641.82 eV and 653.53 eV, corresponding to Mn-2p3/2 and Mn-2p1/2. The spin-orbit split between the Mn-2p3/2 and Mn-2p1/2 levels is 11.7 eV, which means that the manganese oxide supported on the activated carbon is MnO_2. This is in good agreement with the manganese ore characterization results reported by other scholars (Foord et al. 1984). In Fig. 13c, it is clear that there are two separate 2p orbital states at 710.26 eV and 723.76 eV, respectively: Fe-2p3/2 and Fe-2p1/2. The results of the characterization show that the main forms of iron ions supported on the activated carbon are Fe^{3+} and Fe^{2+}, in which results are similar to those reported by other scholars (Singh et al. 2015).

FTIR spectroscopy analysis

As is seen from Fig. 14, the peaks at 1631 cm^{-1} and 3417 cm^{-1} are the absorption peaks of the H–O–H bending vibration (Krehula et al. 2002). These absorption bands are usually produced by the presence of moisture (water vapor). This shows that the prepared Fe-Mn/AC catalyst has a porous structure and can absorb water from the environment. The peak at 2362 cm^{-1} is caused by carbonyl vibration. The stretching vibration peak near 472 cm^{-1} is due to the presence of MnO_2 (Singh et al. 2010). The infrared spectrum of Fe_2O_3 exhibits a stretching peak at a wavelength of 560 cm^{-1} and

790 cm^{-1}, and the infrared spectrum of FeO shows stretching peaks at a wavelength around 670 cm^{-1}. Figure 14 shows stretching peaks at 562 cm^{-1}, 790 cm^{-1}, and 669 cm^{-1}. The results show that the activated carbon has successfully been loaded with iron oxides and manganese oxides. In addition, absorption peaks appear in the infrared spectrum near 1032 cm^{-1} and 1385 cm^{-1}. According to the study (Gomez-Serrano et al. 1996), the absorption peaks appearing here were due to the presence of –C–O and C–O, respectively. The main reason may be that MnO_2 and Fe_2O_3 react with activated carbon during the loading process to promote the formation of these oxidized functional groups.

Concluding remarks

Leachate biochemical effluent was treated using the Fe-Mn/AC-catalyzed $O_3/Na_2S_2O_8$ system, with Fe-Mn/AC as a heterogeneous catalyst. The experimental results proved that it is an efficient and promising method for the treatment of leachate biochemical effluent. The ·OH produced by O_3 and the SO_4^{-}· formed by the activation of $Na_2S_2O_8$ could synergistically oxidize and degrade the pollutants in the wastewater sample, and the two had significant synergistic benefits. The COD and color removal efficiency reached 84% and 98%, respectively. After treatment with the coupling system, the fluorescence index of organic matter ($f_{450/500}$) increased, the fluorescence intensity of organic matter, aromaticity of soluble humic acid decreased, and aromatic ring structure of soluble humic acid are all decreased. Alkane olefins, benzenes, amides, and alcohols were effectively treated, and reactions such as ring opening and chain structure cleavage occurred during oxidation.

The characterization results of the catalyst indicated that the microscopic morphology of the catalyst was porous. The main active component of the catalyst consisted of amorphous MnO_2 and multivalent iron oxides, and the main metal ion components were Mn^{+}, Fe^{2+}, and Fe^{3+}. Moreover, the XRD pattern showed that the diffraction peaks of the metal in the XRD pattern were significantly weakened after Fe and Mn were loaded. This indicated that the Mn and Fe components loaded on the activated carbon were more dispersed than the Mn and Fe in the single-metal-loaded activated carbon. In addition, the Fe-Mn/AC catalyst exhibited strong recyclability, and the treatment efficiency was still 79% after being used four times.

Funding information This work was supported by the National Natural Sciences Foundation of China (Nos. 51468016 and 61640217) and the Technology Development Research Project of Jiangxi (No. 200171BBH80008).

Compliance with ethical standards

Conflict of interest The authors declare that they have no conflict of interest.

References

Abood AR, Jianguo B, Jiangkun D, Dan Z, Ye L (2014) Non-biodegradable landfill leachate treatment by combined process of agitation, coagulation, SBR and filtration. Waste Manag 34:439–447

Ahmed FN, Lan CQ (2012) Treatment of landfill leachate using membrane bioreactors: a review. Desalination 287:41–54

Akhtar J, Amin NS, Aris A (2011) Combined adsorption and catalytic ozonation for removal of sulfamethoxazole using Fe 2 0 3/Ce0 2 loaded activated carbon. Chem Eng J 170:136–144

Amor C, Torres-Socías ED, Peres JA, Maldonado MI, Oller I, Malato S, Lucas MS (2015) Mature landfill leachate treatment by coagulation/flocculation combined with Fenton and solar photo-Fenton processes. J Hazard Mater 286:261–268

Amr SSA, Hamidi Abdul A, Mohd Nordin A (2013) Optimization of stabilized leachate treatment using ozone/persulfate in the advanced oxidation process. Waste Manag 33:1434–1441

An D, Westerhoff P, Zheng M, Wu M, Yang Y, Chiu CA (2015) UV-activated persulfate oxidation and regeneration of NOM-saturated granular activated carbon. Water Res 73:304–310

Baker A (2002) Fluorescence properties of some farm wastes: implications for water quality monitoring. Water Res 36:189–195

Bokare AD, Choi W (2014) Review of iron-free Fenton-like systems for activating H 2 O 2 in advanced oxidation processes. J Hazard Mater 275:121–135

Bourgin M et al (2017) Effect of operational and water quality parameters on conventional ozonation and the advanced oxidation process O3/H2O2: kinetics of micropollutant abatement, transformation product and bromate formation in a surface water. Water Res 122:234

Broséus R, Vincent S, Aboulfadl K, Daneshvar A, Sauvé S, Barbeau B, Prévost M (2009) Ozone oxidation of pharmaceuticals, endocrine disruptors and pesticides during drinking water treatment. Water Res 43:4707–4717

Calabrò PS, Gori M, Lubello C (2015) European trends in greenhouse gases emissions from integrated solid waste management. Environ Technol 36:2125–2137

Calabrò PS, Gentili E, Meoni C, Orsi S, Komilis D (2018) Effect of the recirculation of a reverse osmosis concentrate on leachate generation: a case study in an Italian landfill. Waste Manag S0956053X18301491

Carabineiro SA, Mckee DW, Silva IF (2001) Uncatalysed and catalysed CO2 reaction using metal catalysts and binary vanadium mixtures supported on activated carbon. Carbon 39:451–463

Chemlal R et al (2014) Combination of advanced oxidation and biological processes for the landfill leachate treatment. Ecol Eng 73:281–289

Clarke BO, Anumol T, Barlaz M, Snyder SA (2015) Investigating landfill leachate as a source of trace organic pollutants. Chemosphere 127:269–275

Cortez S, Teixeira P, Oliveira R, Mota M (2010) Ozonation as polishing treatment of mature landfill leachate. J Hazard Mater 182:730–734

Devi P, Das U, Dalai AK (2016) In-situ chemical oxidation: principle and applications of peroxide and persulfate treatments in wastewater systems. Sci Total Environ 571:643–657

Dhaka S, Kumar R, Khan MA, Paeng KJ, Kurade MB, Kim SJ, Jeon BH (2017) Aqueous phase degradation of methyl paraben using UV-activated persulfate method. Chem Eng J 321:11–19

Feng YJ, Li XY (2003) Electro-catalytic oxidation of phenol on several metal-oxide electrodes in aqueous solution. Water Res 37:2399–2407

Foord JS, Jackman RB, Allen GC (1984) An X-ray photoelectron spectroscopic investigation of the oxidation of manganese. Philos Mag A 49:657–663

Forni L, Bahnemann D, Hart EJ (1982) Mechanism of the hydroxide ion-initiated decomposition of ozone in aqueous solution. J Phys Chem 86:255–259

Gao F, Li Y, Xiang B (2018) Degradation of bisphenol A through transition metals activating persulfate process. Ecotoxicol Environ Saf 158:239–247

Gomez-Serrano V, Pastor-Villegas J, Perez-Florindo A, Duran-Valle C, Valenzuela-Calahorro C (1996) FT-IR study of rockrose and of char and activated carbon. J Anal Appl Pyrolysis 36:71–80

Guangxia QI, Yue D, Nie Y (2012) Characterization of humic substances in bio-treated municipal solid waste landfill leachate. Front Environ Sci Eng 6:711–716

Hu L et al (2017) Organic matters removal from landfill leachate by immobilized Phanerochaete chrysosporium loaded with graphitic carbon nitride under visible light irradiation. Chemosphere 184: 1071

Jo YH, Do S-H, Kong S-H (2014) Persulfate activation by iron oxide-immobilized MnO2 composite: identification of iron oxide and the optimum pH for degradations. Chemosphere 95:550–555

Keykavoos R, Mankidy R, Ma H, Jones P, Soltan J (2013) Mineralization of bisphenol A by catalytic ozonation over alumina. Sep Purif Technol 107:310–317

Krehula S, Popović S, Musić S (2002) Synthesis of acicular α-FeOOH particles at a very high pH. Mater Lett 54:108–113

Kumiawan TA, Lo WH, Chan GYS (2006) Radicals-catalyzed oxidation reactions for degradation of recalcitrant compounds from landfill leachate. Chem Eng J 125:35–57

Lee YC, Lo S-L, Chiueh P-T, Liou Y-H, Chen M-L (2010) Microwave-hydrothermal decomposition of perfluorooctanoic acid in water by iron-activated persulfate oxidation. 44:0–892

Leenheer JA, Jean-Philippe C (2003) Characterizing aquatic dissolved organic matter. Environ Sci Technol 37:18A

Legube B, Leitner NKV (1999) Catalytic ozonation: a promising advanced oxidation technology for water treatment. Catal Today 53: 61–72

Li B, Li L, Lin K, Zhang W, Lu S, Luo Q (2013) Removal of 1,1,1-trichloroethane from aqueous solution by a sono-activated persulfate process. Ultrason Sonochem 20:855–863

Liu ZP, Wu WH, Shi P, Guo JS, Cheng J (2015) Characterization of dissolved organic matter in landfill leachate during the combined treatment process of air stripping, Fenton, SBR and coagulation. Waste Manag 41:111–118

Liu M, Zhang L, Xi B-d, Yu S, Hou L-a (2017) Degradation of ciprofloxacin by TiO2/Fe2O3/zeolite catalyst-activated persulfate under visible LED light irradiation. RSC Adv 7:51512–51520

Ma C, He Z, Jia S, Zhang X, Hou S (2018) Treatment of stabilized landfill leachate by Fenton-like process using Fe3O4 particles decorated Zr-pillared bentonite. Ecotoxicol Environ Saf 161:489–496

Matzek LW, Carter KE (2016) Activated persulfate for organic chemical degradation: a review. Chemosphere 151:178–188

Miao D, Peng J, Zhou X, Qian L, Wang M, Zhai L, Gao S (2018) Oxidative degradation of atenolol by heat-activated persulfate: kinetics, degradation pathways and distribution of transformation intermediates. Chemosphere 207:174

Mohamed MA, Jaafar J, Ismail AF, Othman MHD, Rahman MA (2017) Fourier transform infrared (FTIR) spectroscop. 45:3–29

Nawaz F, Xie Y, Xiao J, Cao H, Li Y, Zhang D (2016) Insights into the mechanism of phenolic mixture degradation by catalytic ozonation with a mesoporous Fe3O4/MnO2 composite. RSC Adv 6:29674–29684

Nawrocki J, Fijołek L (2013) Catalytic ozonation—effect of carbon contaminants on the process of ozone decomposition. Appl Catal B Environ 142-143:307–314

Postacchini L, Ciarapica FE, Bevilacqua M (2018) Environmental assessment of a landfill leachate treatment plant: impacts and research for more sustainable chemical alternatives. J Clean Prod 183:1021–1033

Renou S, Givaudan JG, Poulain S, Dirassouyan F, Moulin P (2008) Landfill leachate treatment: review and opportunity. J Hazard Mater 150:468–493

Salari D, Niaei A, Aber S, Rasoulifard MH (2009) The photooxidative destruction of C.I. basic yellow 2 using UV/S2O8(2-) process in a rectangular continuous photoreactor. J Hazard Mater 166:61–66

Saputra E, Muhammad S, Sun H, Ang HM, Tadé MO, Wang S (2013) A comparative study of spinel structured Mn3O4, Co3O4 and Fe3O4 nanoparticles in catalytic oxidation of phenolic contaminants in aqueous solutions. J Colloid Interface Sci 407:467–473

Singh SP, Chakradhar RPS, Rao JL, Karmakar B (2010) EPR, FTIR, optical absorption and photoluminescence studies of Fe2O3 and CeO2 doped ZnO–Bi2O3–B2O3 glasses. J Alloys Compd 493: 256–262

Singh A, Singh A, Singh S, Tandon P, Yadav BC, Yadav RR (2015) Synthesis, characterization and performance of zinc ferrite nanorods for room temperature sensing applications. J Alloys Compd 618: 475–483

Soubh A, Mokhtarani N (2016) The post treatment of composting leachate with a combination of ozone and persulfate oxidation processes. RSC Adv 6:76113–76122

Stefania B, Calabrò PS, Rosa G, Nicola M (2018) Selective removal of heavy metals from landfill leachate by reactive granular filters. Sci Total Environ 644:335–341

Tusar NN et al (2012) Manganese functionalized silicate nanoparticles as a Fenton-type catalyst for water purification by advanced oxidation processes (AOP). Adv Funct Mater 22:820–826

Urs VG (2003) Ozonation of drinking water: part I. Oxidation kinetics and product formation. Water Res 37:0–1467

Wolfe AP, Kaushal SS, Fulton JR, McKnight DM (2002) Spectrofluorescence of sediment humic substances and historical changes of lacustrine organic matter provenance in response to atmospheric nutrient enrichment. Environ Sci Technol 36:3217–3223

Yan J, Khoo E, Sumboja A, Lee PS (2010) Facile coating of manganese oxide on tin oxide nanowires with high-performance capacitive behavior. ACS Nano 4:4247–4255

Yang D, Ezyske CM (2011) Sulfate radical-advanced oxidation process (SR-AOP) for simultaneous removal of refractory organic contaminants and ammonia in landfill leachate. Water Res 45:6189–6194

Zhang QQ, Tian B-H, Zhang X, Ghulam A, Fang C-R (2013) He R Investigation on characteristics of leachate and concentrated leachate in three landfill leachate treatment plants. Waste Manag 33: 2277–2286

Zhang Y, Zhang Q, Dong Z, Wu L, Hong J (2018) Structural modified CuFe 2O4/persulfate process for acetaminophen scavenging: high efficiency with low catalyst addition. J Chem Technol Biotechnol 94

Zhao Z et al (2017) Advanced oxidation removal of hypophosphite by O3/H2O2 combined with sequential Fe(II) catalytic process. Chemosphere 180:48–56

Zheng Z, He P-J, Shao L-M, Lee D-J (2007) Phthalic acid esters in dissolved fractions of landfill leachates. Water Res 41:4696–4702

Zhou L, Cao H, Descorme C, He Z, Xie Y (2018) Wet air oxidation of indole, benzopyrazole, and benzotriazole: effects of operating conditions and reaction mechanisms. Chem Eng J 338:496–503

Zhu L, Qi H-y, Lv M-l, Kong Y, Yu Y-w, Xu X-y (2012) Component analysis of extracellular polymeric substances (EPS) during aerobic sludge granulation using FTIR and 3D-EEM technologies. Bioresour Technol 124:455–459